Bulk plasma properties in the pulsed glow discharge

Glen P. Jackson[a], Fred L. King[b],*

[a]*Chemical Sciences Division, Oak Ridge National Laboratory, P.O. Box 2008, Oak Ridge, TN 37831-6375, USA*
[b]*Department of Chemistry, West Virginia University, Morgantown, WV 26506-6045, USA*

Abstract

This work focuses on the spatial and temporal characteristics of a glow discharge plasma operated with power pulses of 5 ms in duration at 25% duty cycle. Interpretation of emission data provides insight into the nature of the plasma at each instant of a typical pulse cycle and at each position in space. Because the bulk plasma properties affect the distribution of excited energy levels of the sputtered atoms, an improved understanding of the plasma affords the ability to select conditions that enhance analytically important emission lines. Optical emission spectroscopy was used to determine the relative populations of excited states for atoms and ions during the initial breakdown, the steady state and the recombining periods of the discharge pulse cycle. The plasma is highly ionizing in nature at the time of breakdown—with lower excited states being overpopulated—before reaching the steady state, or plateau, period, also ionizing in nature. These behaviors arise from a loss of charged particles and photons to the surroundings that shifts the plasma away from Saha and Boltzmann balances during these periods. The post-pulse period typically displays recombining behavior, characterized by population inversion for selected species—except for regions close to the cathode, where electrons and ions are lost by diffusion and are not available for recombination. The sputtered analyte atom emissions closely mimic those of the plasma bath gas, except that their emissions persevere for longer in the recombining after-peak period than do the discharge gas species.
© 2003 Elsevier Science B.V. All rights reserved.

Keywords: Pulsed glow discharge; Ionizing plasma; Recombining plasma; Atomic emission; Transient plasma

1. Introduction

Glow-discharge mass spectrometry (GDMS) is a versatile, simple and robust technique for the analysis of conducting and non-conducting solids [1–7]. For analytical applications, research has shown that operation of glow discharge plasmas with micro-millisecond duration pulsed power affords many advantages over steady-state operation [8–13]. This not only enables higher instantaneous power to be used, resulting in increased sputtering, excitation and ionization, but also allows the use of gated detection to achieve maximum analytical performance and versatility [10]. This versatility includes the ability of these sources to be extended to use in chemical speciation as well as elemental analysis [14].

In order to exploit fully the advantages of pulsed glow discharge sources (PGDs), a fundamental

*Corresponding author. Tel.: +1-304-293-4611; fax: +1-304-293-4904.
E-mail address: fred.king@mail.wvu.edu (F.L. King).

understanding of the excitation and ionization phenomena occurring throughout the various temporal and spatial domains of the plasma is required. The spatial and temporal characteristics of metastable argon atoms and sputtered copper species in these plasmas have been presented in previous reports from this laboratory [15–17]. Because these species account for only a small fraction of the total plasma composition, knowledge of the spatio-temporal fluctuations in excitation and ionization for the argon discharge gas is required to understand the bulk behavior of the plasma. Such an understanding enables complete utilization of the many advantages of PGDs [18]. The present study focuses on the evolution of plasma processes and energetics over a typical pulse cycle as they relate to the generation of analyte signals.

Although much effort has been expended in understanding the fundamental processes occurring in steady-state glow discharges [19–29], the same level of understanding has not yet been realized for pulsed glow discharges [30,31]. Some previous effort was made to characterize the emission and ionization characteristics of PGDs. Duncen et al. [32] observed an increase in emission from argon atoms following power termination in a pulsed glow discharge and suspected that contaminated gases played some role in this process. Strauss et al. [33] reported that the emission intensity of selected wavelengths in the after-peak nearly doubled that found in the plateau. These after-peak emissions could also be reduced by the addition of methane because of its quenching effect on the metastable argon atoms.

Like any other plasma, the GD plasma mainly consists of ground-state argon atoms, excited-state neutrals (including metastable states), and ground- and excited-state argon ions of various charge states, electrons and photons. On a microscopic level, these species are in a constant state of flux as energy is continually exchanged among them through various interactions. If every process that occurs in the plasma is fully reversible, the plasma is said to be in a state of thermodynamic equilibrium (TE) and the description of the plasma is relatively simple [34]. The macroscopic state of the plasma can be fully described by various statistical models that govern the distribution of

energy levels in the plasma. In TE, the equations of Maxwell, Boltzmann, Saha and Planck fully describe the velocity distribution, the excited state distribution, the degree of ionization and the transfer of photons, respectively. Significantly, all of these processes are balanced, permitting the energy for a plasma in TE to be defined by a single temperature. If, for any reason, a given process ceases to be perfectly reversible—for example, if particles are lost to the chamber walls—the plasma will cease to be in equilibrium and its statistical description becomes much more difficult [34–39].

PGDs do not display TE [40] because the proper forward and reverse reactions do not always balance. For example, ions diffuse to the chamber walls and initially disrupt the Saha balance. This deviation from equilibrium consequently impacts the Boltzmann and Planck distributions, because excited state neutrals are no longer formed by recombination reactions. Because of the various ways in which plasmas can deviate from ideality, a more detailed understanding of the balances and relations that do occur in PGDs is necessary to understand how they behave. Such an understanding is useful in determining how they can be exploited for greater analytical benefit. This paper provides an abbreviated account of investigations towards this end—an extended version of which appears elsewhere [41].

2. Experimental

The experimental apparatus used in this study is described in detail elsewhere [15,42]. A stainless steel six-way cross housed the direct insertion probe, onto which sample cathode disks were mounted. A copper disk (NIST SRM 495, Gaithersburg, MD) of 4.0 mm in diameter was used as the cathode. A translation platform held the six-way cross and could be moved orthogonal (in the x-dimension) to the monochromator to permit observations of different regions of the plasma. The direct insertion probe also maneuvered orthogonal to the monochromator (in the y-dimension) to alter the sampling distance above the cathode. In this way, two-dimensional emission maps could be obtained for each line.
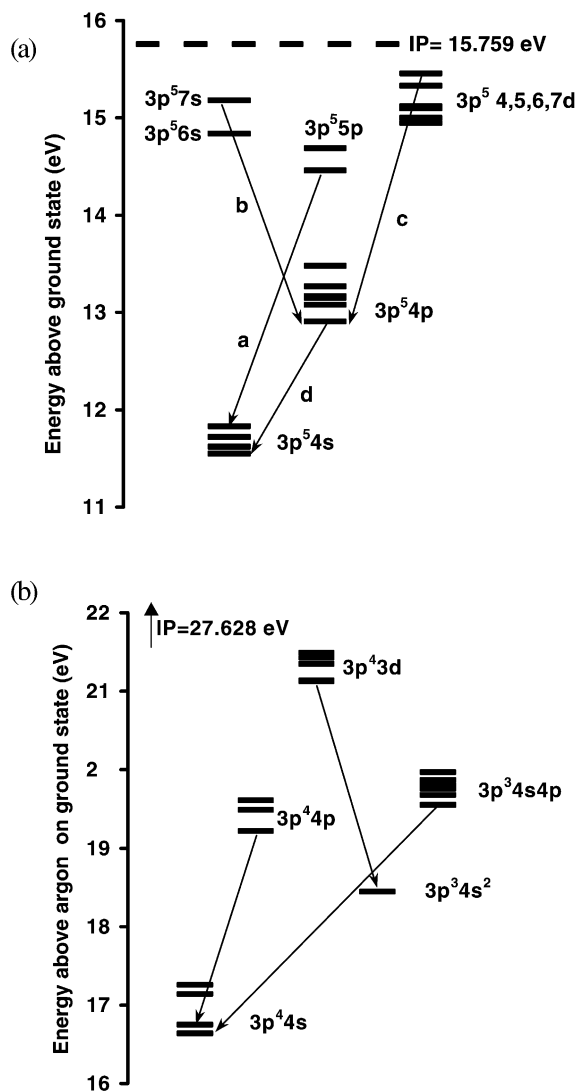
Fig. 1. Energy level diagrams showing the lines of interest for the various states of the argon (a) atom and (b) ion.

Operating conditions were as follows: argon discharge gas, 0.8 torr; peak current, 1.6 mA; and applied voltage, ~860 V. The emission from the discharge cell was imaged in a 1:1 ratio on the entrance slit of the monochromator. Entrance and exit slits were 50 μm wide and 1.0 mm high. The extended-red photomultiplier tube (R-928, Hamamatsu, Bridgewater, NJ) operated at 800 V, unless otherwise stated. Data acquisition was accom-

plished as described in previous reports from this laboratory [15,16].

Fig. 1a,b shows energy level diagrams for selected argon atom and ion states, respectively. The individual emission lines studied are given in Tables 1 and 2. The argon atom lines are classified into groups according to the manifolds from which they originate. These groups are labeled as a–d on the energy level diagram in Fig. 1.

3. Results and discussion

3.1. Argon atom emission

Fig. 2 shows the temporal emission profiles for four selected argon emission lines, representative of the general behavior observed for the other transitions between the manifolds shown in Fig. 1a. The effects of sampling height demonstrate the inhomogeneity of the plasma and the need to make diagnostic measurements parallel to the cathode surface, 'side-on'.

Table 1
Spectroscopic data for argon atom lines examined in this study

Wavelength (Å)	Transition probability A (10^8 s^{-1}) [83]	Energy levels (eV)		Statistical weight	
		E_L	E_U	g_L	g_U
4200.7	0.010	11.55	14.46	5	7
4333.6	0.006	11.83	14.69	3	5
5373.5	0.003	13.15	15.46	3	5
5495.9	0.017	13.08	15.33	7	9
5650.7	0.032	12.91	15.10	3	1
5888.6	0.013	13.08	15.18	7	5
5912.1	0.011	12.91	15.00	3	3
6664.1	0.002	13.09	14.95	5	5
6719.2	0.002	13.27	15.12	1	3
7503.9	0.445	11.83	13.48	3	1
7514.7	0.402	11.62	13.27	3	1
7635.1	0.245	11.55	13.17	5	5
7723.8	0.052	11.55	13.15	5	3
8115.3	0.331	11.55	13.08	5	7

E_L and E_U refer to the lower and upper energy levels of the states, respectively; g_L and g_U refer to the lower and upper statistical weights, respectively.

Table 2
Spectroscopic data for argon ion lines examined in this study

Wavelength (Å)	Transition probability A (10^8 s^{-1}) [83]	Energy levels (eV)		Statistical weight	
		E_L	E_U	g_L	g_U
4131.7	1.4	18.43	21.43	4	2
4277.5	0.41	18.45	21.35	4	6
4331.2	0.56	16.75	19.61	4	4
4348.1	1.24	16.64	19.49	6	8
4370.8	0.65	18.66	21.49	4	4
4401.0	0.322	16.41	19.22	8	6
4426.0	0.83	16.75	19.55	4	6
4545.1	0.413	17.14	19.87	4	4
4590.0	0.82	18.43	21.13	4	6
4609.6	0.91	18.45	21.14	6	8
4657.9	0.81	17.14	19.80	4	2
4726.9	0.5	17.14	19.76	4	4
4764.9	0.575	17.26	19.87	2	4
4806.0	0.79	16.64	19.22	6	6
4879.9	0.78	17.14	19.68	4	6
4965.1	0.347	17.26	19.76	2	4

3.1.1. $3p^55p–3p^54s$ transitions (Fig. 2a and Fig. 3a)

These 'blue' lines result in the population of four possible states. Transitions involving two of these states, $(^1s_2)$ $^1P_1$ and $(^1s_4)$ $^3P_1$, are resonant with the ground state and are too short in wavelength to be observed with the apparatus employed. Transitions between the remaining states, $(^1s_3)$ $^3P_0$ and $(^1s_5)$ $^3P_2$, and the ground state are spin-forbidden and are therefore metastable [43]. Under the operating conditions used here, approximately 30–50% of the metastable argon atoms are thought to form via radiative decay from the 5p level [21] and their lifetime is of the order of 1–10 ms [44,45]. Emission from such transitions, populating the metastable states, gives a good indication of the spatial location of these metastable argon atom populations in the plasma.

The temporal profiles of emission intensity at 420.07 nm ($5p[2^1/_2]–4s[1^1/_2]$, 14.50–11.55 eV) are plotted in Fig. 2a for various observation points. The emission intensity as a function of distance is presented in Fig. 3a. The maximum emission intensity over the entire pulse cycle is
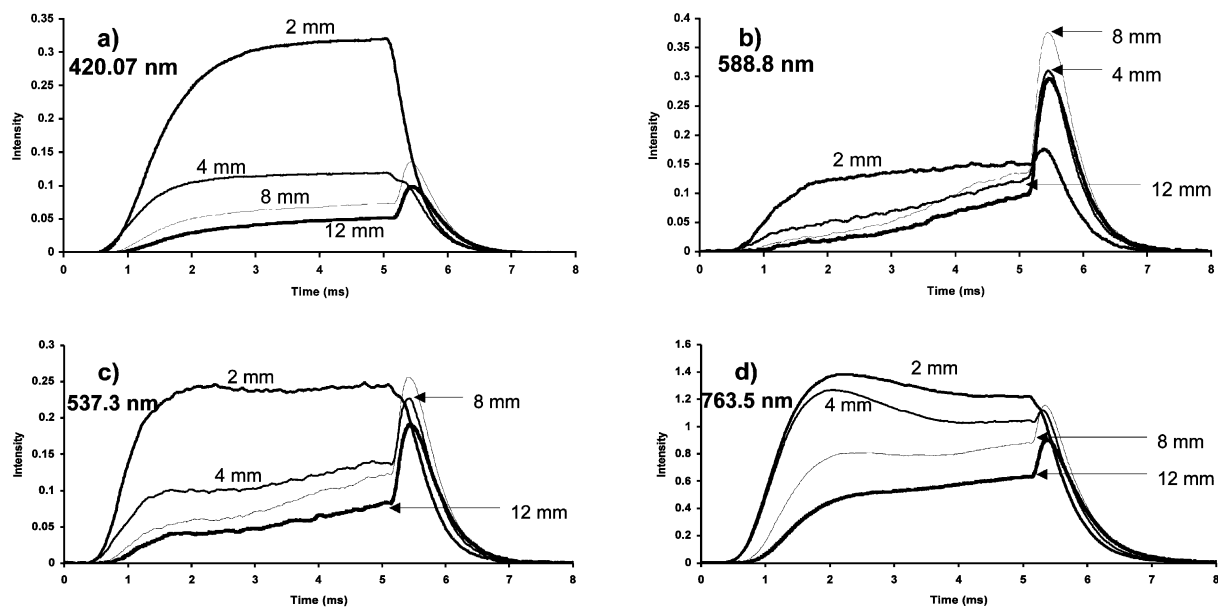

Fig. 2. Temporal traces for selected argon atom transitions at different distances above the cathode; (a–d) refer to the labels in Fig. 1a. Pulse length, 5.0 ms; Ar pressure, 0.8 Torr; peak power, ~1.5 W.
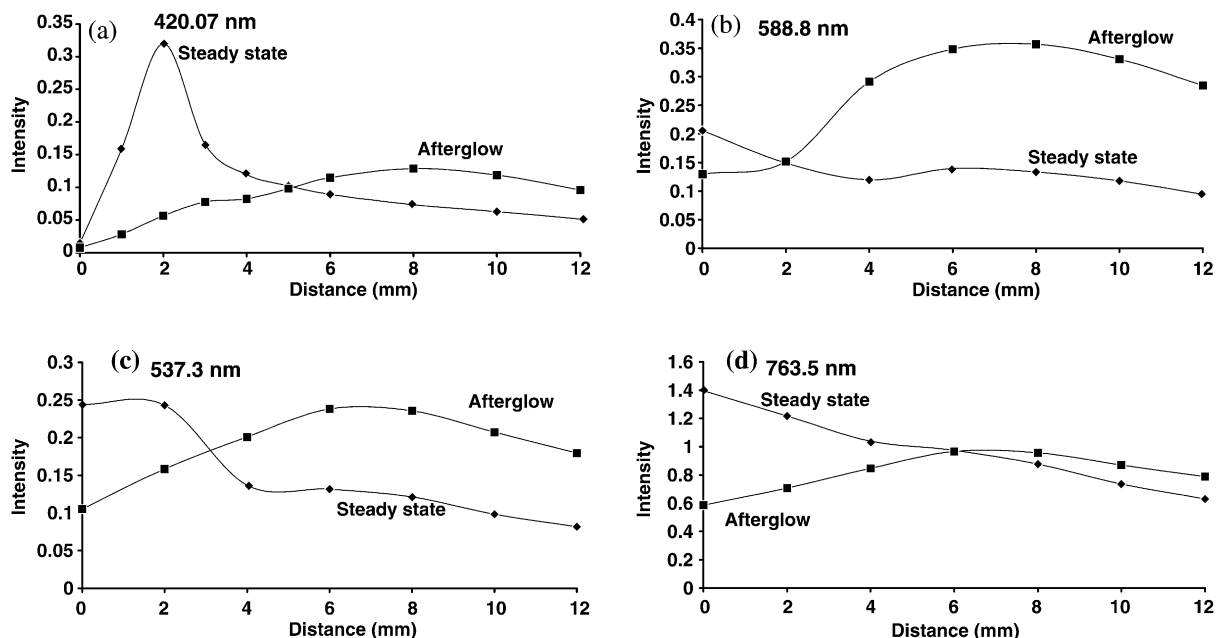
Fig. 3. Optical emission signals for argon atom lines in the steady state (*diamonds*) and after-peak (*squares*) as a function of distance; (a–d) refer to the labels in Fig. 1a. Pulse length, 5.0 ms; Ar pressure, 0.8 Torr; peak power, ∼1.5 W.

found at 2.0 mm above the cathode during power application. The maximum emission intensity during the voltage-on period decreases dramatically from 2.0 to 4.0 mm, and decreases in a linear fashion at greater distances. Comparable behavior was observed by Rózsa and Gallagher for a similar transition in a steady-state glow discharge [19]. The behavior is attributed to the method of 5p level population: close to the cathode, excitation is by fast atom/ion collisions, whereas in the negative glow it is predominantly by electron excitation. Upon power termination, little or no after-peak is observed between 0 and 2 mm. The lack of an after-peak close to the cathode can be attributed to one or both of the following possibilities: (i) electrons do not play a significant role in populating these states while the discharge is on. If electrons did populate these levels, the sudden decrease in electron temperature in the after-peak would be expected to cause a 'Saha jump' in the after-peak [46–48]. (ii) Electrons are not available for recombination in the after-peak because they are lost to the cathode surface.

When the plasma is extinguished a surge in the emission intensity is observed for this line at distances beyond 2.0 mm. Fig. 3a shows that the after-peak intensity maximizes at ∼8 mm at this pressure. The emission maximum in the after-peak appears at ∼350 μs under these conditions. The time delay between voltage termination and the beginning of emission is related to the time required for the fast electrons to thermalize via collisions [49,50]. This is thought to occur very rapidly at pressures of ∼10–760 torr—of the order of 1 μs or less [49,51], but takes longer—on the order of 100 μs—at lower pressures [52]. Recombination is also more probable further from the cathode because the argon ion population, which is predominantly formed in the negative glow, is greatest between 4 and 8 mm [53,54]. The after-peak maximum shifted to slightly longer times (by 10–20 μs) at 16–20 mm from the cathode, indicating that the electron temperature may take slightly longer to decrease at these long distances. The emission decay rates occurring after the after-

peak maximum are discussed in more detail in Section 3.6.

3.1.2. $3p^5 7s$–$3p^5 4p$ transitions (Fig. 2b and Fig. 3b)

It can be observed from the temporal profile presented in Fig. 2b that the emission intensity at 588.86 nm ($7s[1^1/_2]$–$4p[2^1/_2]$, 15.18–13.08 eV) reaches a steady-state value close to the cathode surface, but not at distances beyond 2.0 mm from the surface. Because all the transitions involving an upper energy level of 15 eV or higher showed this behavior, we might expect that above 2 mm a stepwise mechanism is responsible for populating these high levels. Indeed, Bogaerts and co-workers reported that the electron excitation from already-excited levels increases in importance for populating these higher levels [21,55]. At 5.0 ms the intensity reaches a maximum in the negative glow at ∼6 mm. Bogaerts et al. predicted that this population occurs ∼2 mm above the cathode in a 1.0-torr plasma [55]. The present observation, at 0.8 torr, is reasonably consistent with the model when the pressure difference is taken into account.

At distances closer than 2.0 mm to the cathode, the emission intensity for the 588.86 nm line decays rapidly upon power termination. No after-peak is evident in the temporal profiles (for reasons discussed in Section 3.1.1). Further from the cathode, however, a significant increase in after-peak emission is observed (see Fig. 2b). The maximum intensity of the after-peak is also found between 6 and 8 mm. The after-peak/plateau emission intensity ratio is much larger for this transition than for the 5p–4s transitions.

Distance profiles of the emission intensity at 588.86 nm for the 7s–4p transition during plateau (diamonds) and in the after-peak (squares) in Fig. 3b show behavior not easily discerned from the temporal profiles of Fig. 2a. Power application generates maxima in the populations at two spatial positions. One maximum is at the cathode surface, where fast atom/ion collision is the dominant excitation mechanism [19,26,56]. The other maximum is found at ∼6 mm above the cathode, where electron excitation dominates. Relative to the emission at 420.07 nm, the cathode darkspace/ negative glow intensity ratio is much smaller for

this transition. This indicates the smaller probability of accessing this higher-energy 7s state via fast atom/ion collisions than the lower-energy 5p and 4p states.

3.1.3. $3p^5 4$–$7d$–$3p^5 4p$ transitions (Fig. 2c and Fig. 3c)

The transitions of this manifold are typified by the temporal emission profiles shown in Fig. 2c for the $7d[2^1/_2]$–$4p[^1/_2]$ (14.46–13.15 eV) transition at 537.35 nm. As observed from the data presented in Fig. 2c and Fig. 3c, the after-peak/ steady-state emission ratio is also slightly less for this transition than that observed for the 7s–4p transition (Fig. 2b and Fig. 3b) described in the previous section. In the distance profile (Fig. 3c) it is evident that during the plateau the emission intensity maximizes at the cathode surface. A much smaller maximum is also evident in the negative glow at 6 mm, indicating that fast atom/ ion collisions are a slightly more significant mechanism of populating these levels. Indeed, reports published indicate that higher-energy electronic orbitals have a smaller probability of being formed via fast atom/ion collisions [56]. Because the 7d state has a slightly lower energy than the 7s state, fast atom/ion excitation causes the cathode dark-space/negative glow emission intensity for transitions from the 7d state to be greater than that for transitions from the 7s state.

3.1.4. $3p^5 4p$–$3p^5 4s$ transitions (Fig. 2d and Fig. 3d)

Temporal profiles for the $4p[1^1/_2]$–$4s[1^1/_2]$ transition (13.17–11.55 eV) at 763.51 between 2.0 and 8.0 mm, as observed in Fig. 2d, display a distinct prepeak at ∼2 ms. Because the onset of the pulsed discharge commences with a cascade of electrons, it appears that the 4p levels are preferentially populated by electron excitation mechanisms. Indeed, no prepeak behavior is observed from the 5p levels and they are the next closest in energy to the 4p states.

The distance profile (Fig. 3d) shows that at 5.0 ms the steady-state emission at 763.51 nm reaches a maximum at the cathode surface and then decays almost linearly with increasing distance from the cathode. After-peak emission intensities increase

gradually from a minimum at the cathode surface to a maximum between 6 and 8 mm. Only at distances beyond 6 mm does the after-peak intensity exceed that of the plateau. The notable difference in plateau and after-peak emission intensities for this line, as compared to the previous three lines, illustrates the dramatic differences the emission profiles can assume depending on the upper electronic energy level of the emitting species. This also provides important clues regarding the differences between mechanisms responsible for the population of these different states.

3.2. Argon ion emission

Mass spectrometric studies [16,42,57,58] have shown that argon ion densities are almost negligible 100 μs after pulse termination. It is not surprising, therefore, that their emissions do not prevail in the after-peak [33,42]. In this study it was also found that emission from excited argon ions in Table 2 do not exhibit an after-peak and that the intensity follows an approximate exponential decay after the plasma is extinguished.

All the argon ion transitions observed (not shown) followed almost identical behavior. Maximum emission intensity is reached 2.0 mm above the cathode, whereas the minimum is observed at the surface. This suggests that fast atom/ion collisions do not play a significant role in populating Ar ion states. The emission intensity decreases at distances beyond 2.0 mm from the surface. This behavior is indicative of the electron excitation that dominates the area between 2.0 and 5.0 mm.

3.3. Deviations from thermodynamic equilibrium

All the atom lines observed in this study exhibited some degree of an after-peak at distances beyond 2 mm above the cathode surface. The observation of this surge in emission intensity for all argon atom species can be understood in terms of the shift of the plasma from an ionizing mode during the plateau to a recombining mode during the after-peak. Theoretical evidence for such behavior has been described previously [35–38]. Similarly, the observation of such behavior in other types of plasmas has been reported in the literature

[59]. It is useful to understand now how these phases deviate from the ideal balances predicted by thermodynamic equilibrium (TE).

3.3.1. Departures from Saha and Boltzmann distributions

The Saha balance describes the balance between electron ionization of excited atom states by fast electrons and the three-body recombination of argon ions with two thermal electrons. When the voltage is removed from the PGD plasma, electrons are no longer accelerated by the electric field and the high-energy electrons become thermalized. This shifts the Saha balance downwards in energy via recombination reactions with the concomitant population of highly excited neutral states. If the population of an energy level follows a Saha predicted equilibrium during power application, the response to power termination will be [47,48]:

$$\ln(I'/I) = 3/2\ln\gamma + (E_{\mathrm{ion}} - E_p)\big([\gamma - 1]/kT_{\mathrm{e}}\big) \qquad (1)$$

where I' and I are the emission intensities of a line in the after-peak and steady-state times, respectively, $\gamma = T_{\mathrm{e}}/T_{\mathrm{g}}$, E_{ion} and E_p are the energies of the ion ground state and p-th excited atom level, respectively, and k is Boltzmann's constant. For such plasma in TE, a plot of $\ln(I'/I)$ vs. $(E_{\mathrm{ion}} - E_p)$ should give a straight line with a positive slope of $[\gamma - 1]/kT_{\mathrm{e}}$ and an intercept of $3/2\ln\gamma$ [47], as shown by the dashed line in Fig. 4a. The points in Fig. 4a actually suggest a negative slope with a y-intercept >1. This indicates significant deviation from the Saha balance during the voltage-on period, as expected if the loss of electrons and ions to the surroundings restricts the proper recombination balance.

If population of the argon excited levels follows a Boltzmann distribution, then the natural logarithm of atom emission ratios I'/I plotted as a function of E_p (Fig. 4b) should fall on a straight line with a negative slope of $-(\gamma - 1)/kT_{\mathrm{e}}$ [48]. It is evident from the data that this is not the case. If we treat transitions from the lowest levels (13–13.5 eV) separately, and assume that these could be in Boltzmann balance with the ground state, lines of best fit through these points at each
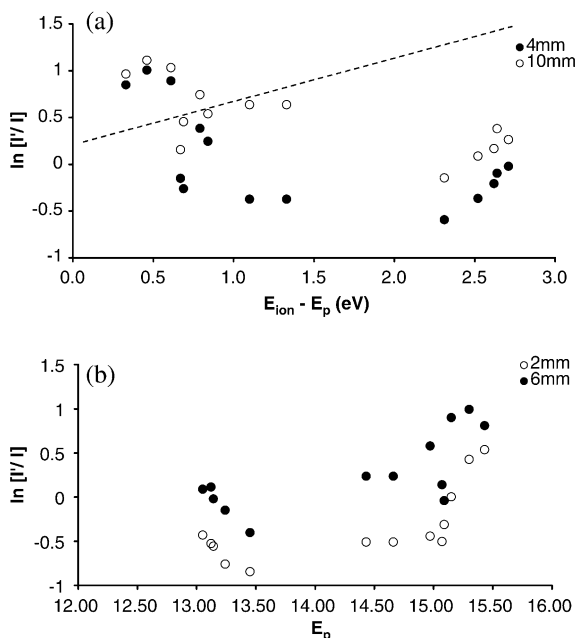
Fig. 4. (a) Plot to determine the electron temperature from the Saha response of argon atom lines to the voltage termination. (b) Plot to determine the electron temperature from the Boltzmann response to voltage termination. The dashed line in (a) signifies where the points might fall if TE or pTE existed, i.e. for an ICP plasma [47,48].

sampling distance reveal electron temperatures of the order of 9500 ± 1500 K above the gas temperature. These temperatures are considerably higher than previous reports of 2000–6000 K, indicating deviation even from partial TE (pTE) [60–64].

Using these same methods, the emission intensity ratios for the copper atom lines given in Table 3 were also employed to determine T_e and the state of TE in the PGD plasma. Fig. 5a compares the excited-state population observed with that predicted by the Saha equation. As was the case for argon emissions, the points do not provide a positive slope. In fact, lines corresponding to transitions from levels within 2 eV of the IP deviate more from the Saha-predicted behavior than do the argon levels in this region. Based on the smaller ionization potential of copper compared to argon, we would expect the copper population to be more highly ionized and therefore more likely to be in agreement with the Saha

equation. Clearly, the data here show that these plasmas deviate significantly from TE conditions, with extensive loss of electrons and ions to the chamber walls.

Fig. 5b is a plot of the copper atom emission intensity ratios used to determine their consistency with the Boltzmann equation. The points do not suggest a negative slope, as predicted for a plasma transitioning from an equilibrium state to one that is dominated by recombination. This can be taken as further evidence that the GD plasma is far from TE conditions when the plasma voltage is termi-

Table 3
Spectroscopic data for the copper atom emission lines examined in this study

| Wavelength (Å)	Transition probability A (10^8 s^{-1}) [83]	Energy levels (eV)		Statistical weight	
		E_L	E_U	g_L	g_U
2238.5		1.64	7.18	8	6
2492.2	0.031	0.00	4.97	2	6
2618.4	0.307	1.39	6.12	6	4
2824.4	0.078	1.39	5.78	6	6
3073.8		1.39	5.42	4	6
3093.9		1.39	5.39	4	8
3194.1	0.016	1.64	5.52	4	4
3247.5	1.390	0.00	3.82	2	4
3273.9	1.370	0.00	3.79	2	2
3279.8		1.64	5.42	4	6
3292.8		1.39	5.15	6	6
3337.9	0.004	1.39	5.10	6	8
3385.4		3.79	7.45	2	4
3414.0		3.82	7.45	4	6
3481.6		3.79	7.35	2	4
3511.8		3.82	7.35	4	6
3530.4		1.64	5.15	4	6
3654.2		3.79	7.18	2	4
3687.4		3.82	7.18	4	6
3825.0		3.79	7.03	2	2
3861.7		3.82	7.03	4	2
4062.6	0.210	3.82	6.87	4	6
4063.2	0.210	3.82	6.87	4	6
4480.3	0.030	3.79	6.55	2	2
5105.5	0.020	1.39	3.82	6	4
5153.2	0.600	3.79	6.19	2	4
5218.2	0.750	3.82	6.19	4	6
5700.2	0.002	1.64	3.82	4	4
5782.1	0.017	1.64	3.79	4	2
7933.1		3.79	5.35	2	2
8092.6		3.82	5.35	4	2
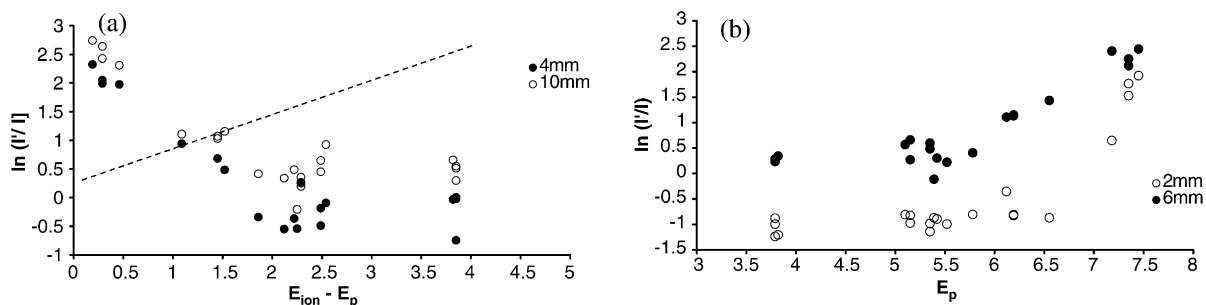
Fig. 5. (a) Plot to determine the electron temperature from the Saha response of copper atom lines to the voltage termination. (b) Plot to determine the electron temperature from the Boltzmann response to voltage termination. The dashed line in (a) signifies where the points might fall if TE or pTE existed, i.e. for an ICP plasma [47,48].

nated at 5 ms. In this case, not even the lower levels of copper approximate to the Boltzmann balance.

Although the Boltzmann and Saha balances have just been shown to be poor descriptors of the population of energy states, other equilibria conditions that are electron density-sensitive can be calculated to determine the distribution of excited states. For example, Fig. 6a shows that if the electron density is below 10^{10} cm^{-3}, excited levels decay to the ground state via radiative transitions rather than by electron de-excitation. Under these circumstances, a Corona balance determines that the distribution of energy states is populated proportionally to $p^{-0.5}$, where p is the principle quantum number [35,36]. At high electron densities ($> 10^{14}$ cm^{-3}) the plasma enters the saturation phase. In this case, ladder-like excitation by electrons continues up the higher levels until the population of energy levels is proportional to p^{-6} [34–36]. For electron densities between these two extremes, i.e. the $\sim 10^{11}$–10^{12} cm^{-3} densities found in typical glow discharges [60,61], the population of energy levels will lie between the extremes of $p^{-0.5}$ and p^{-6} dependence. Regardless of the electron density [65], an ionizing plasma will always have an over-population of lower levels and an under-population of excited levels with respect to an equilibrium plasma defined by the Boltzmann equation.

3.3.2. Additional factors contributing to deviation from TE

As well as the deviation from TE caused by the different forces applied to the different particles in the discharge, and the losses of electrons and ions, there are other factors that add to the departure of GDs from TE. Radiation is lost to the surroundings, so the re-absorption of radiation by lower-excited states will be less than expected. This deviation from the Planck balance also will tend to over-populate the lower energy levels.

The velocity distribution of electrons is known to be non-Maxwellian in steady-state GD sources [1,61], and this contributes strongly to deviations from TE. The non-Maxwellian distribution is primarily caused by the acceleration of electrons by the electric field. Non-Maxwellian behavior is also caused, in part, by ionization reactions that release electrons with high kinetic energy [61]. For example, Penning ionization (PI)

$$Ar^m + M \rightarrow Ar^0 + M^+ + e^- \quad (x \text{ eV}) \tag{2}$$
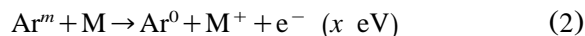
releases electrons with kinetic energy dependent on the IP of M. If M is another metastable argon atom (IP $\approx$ 4.2 eV) the expelled electrons will have $\sim$7.3 eV of kinetic energy. These electrons contribute to the number of high-energy electrons in the electron-energy distribution function (EEDF) and distort the Maxwellian distribution. Penning ionization of the sputtered atoms also contributes
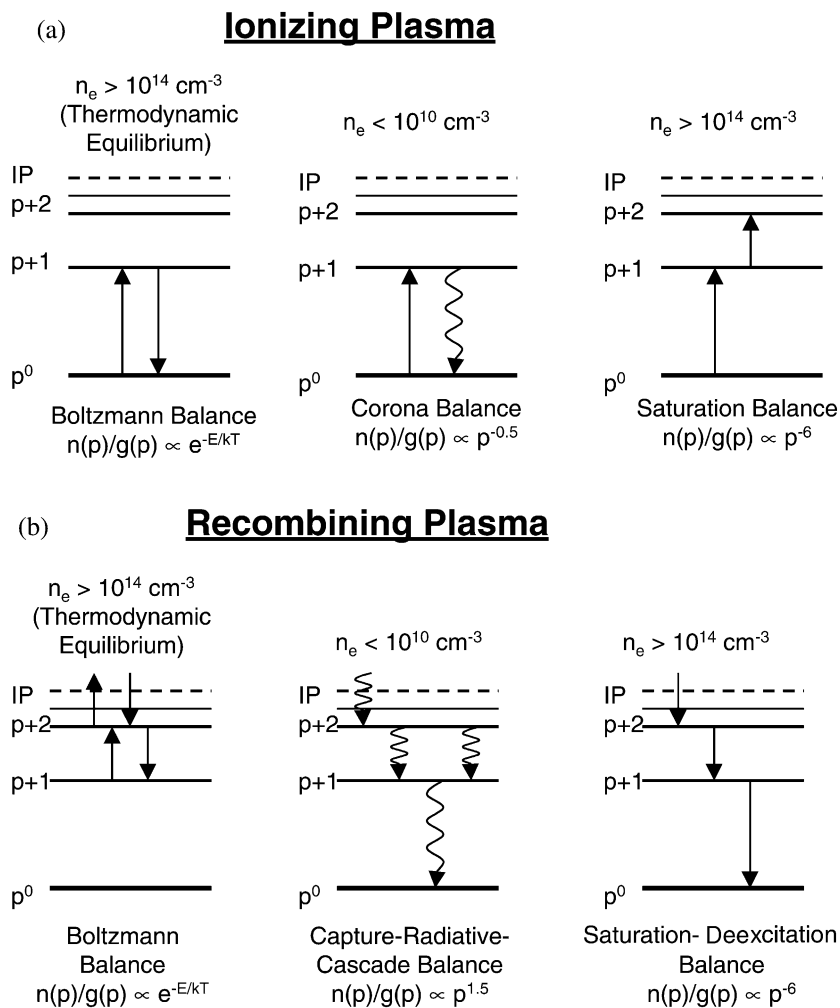
Fig. 6. (a) Examples of electron excitation mechanisms at different electron number densities in an ionizing plasma. Solid lines and wavy lines represent electron and photon-accompanied transitions, respectively. $n(p)/g(p)$ is the population density per unit statistical weight, $p = 0$ is the ground state and IP is the ionization potential. Between 10^{10} and 10^{14} electrons cm^{-3} the Griem and Byron criteria determine which levels of p are governed by which balance [34,37]. Above 10^{14} electrons cm^{-3} the Byron criterion divides the lower levels ($p < 7$) and the upper levels ($p > 10$) into the Boltzmann balance and saturation excitation balance, respectively [34,37]. (b) Examples of electron de-excitation mechanisms at different electron number densities in a recombining plasma. Solid lines and wavy lines represent electron and photon accompanied transitions, respectively.

strongly to the number of high-energy electrons in the plasma. This is demonstrated by the occurrence of higher electron temperature measurements in plasmas having cathode materials with lower ionization potentials [61].

Associative ionization, also known as the Hornbeck–Molnar reaction [66]

$$Ar^* + M \rightarrow ArM^+ + e^- \quad (x \text{ eV}) \qquad (3)$$
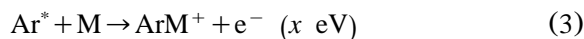
is another mechanism by which the influx of electrons can disrupt the Maxwellian distribution of velocities. If M is a ground-state argon atom, the onset for this reaction occurs at ~ 15 eV, implying that the metastable states are not involved

in this reaction. For metal–noble gas molecular ions [67], however, the metastable states of argon are energetically viable reactants for this mechanism of ionization.

3.4. Phase transitions at the pulse onset

The onset of the pulsed voltage is a time of significant change in the plasma characteristics. Between the initial gas breakdown and the steady-state condition, changes in populations are energy-level-dependent. For example, the emission from the 4p states (see Fig. 2d) demonstrates a significant prepeak, whereas the emission lines for higher levels (i.e. 7s and 4d states in Fig. 2b,c, respectively) show opposite behavior. Their emission intensities are smaller at 2 ms than at 5 ms (at distances >4 mm). The copper atom lines demonstrate similar behavior: lower-energy lines show a pronounced prepeak but emissions from higher energy lines are weaker in the prepeak domain than in the steady state. Lines between the upper and lower levels, i.e. the 5p states, generally reach a steady-state signal quite early in the pulse and do not fluctuate considerably until voltage termination. The initial gas breakdown therefore appears to selectively overpopulate the lower levels and underpopulate the upper levels with the respect to the plateau signals.

Fig. 7 shows the after-peak/steady-state and after-peak/prepeak emission ratios for all the argon lines in Table 1 plotted as a function of the energy of the emitting levels. At 6 and 10 mm above the cathode, the after-peak/prepeak ratios are significantly larger than the after-peak/steady-state ratios for the higher-lying states. This implies that the higher-lying states are considerably less populated in the prepeak than during the steady state. The higher population of the lower levels in the prepeak (as observed for the 4p states, Fig. 2d) stems from the initial conditions of the plasma. At the onset of the voltage, the argon ground state is severely overpopulated and the applied electric field decreases linearly between the cathode and anode. As fast electrons ionize the argon, the charged-particle number density increases until space-charge factors prevent any further increase [26]. Initially, the lowest excited states populate
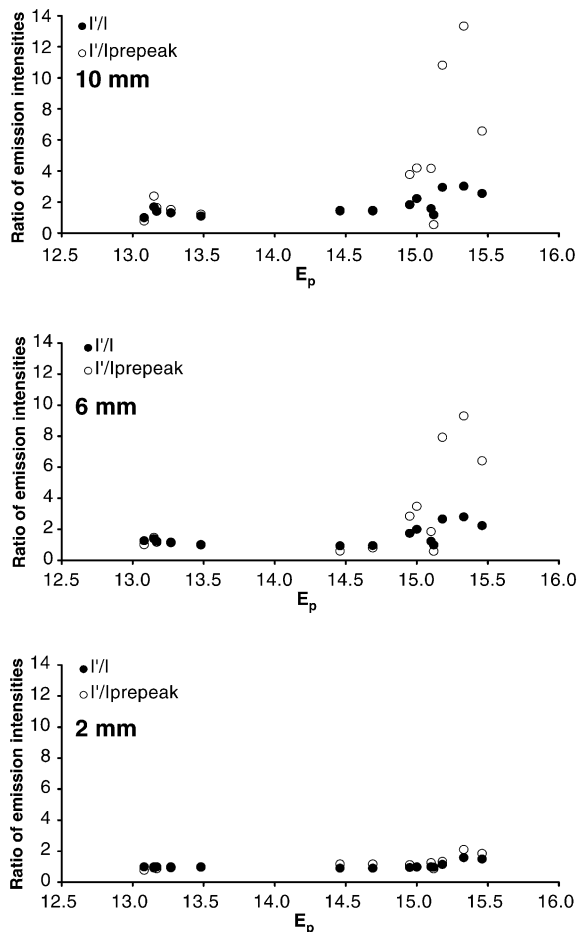

Fig. 7. Plots of the after-peak/steady-state (I'/I) and after-peak/prepeak ($I'/I_{prepeak}$) intensity as a function of the energy level of the emitting level at different sampling distances above the cathode.

via electron excitation from the ground state according to the corona balance, but as the electron number density increases these lower-excited states become overpopulated and subsequently excite to increasingly higher levels according to the saturation balance. The lower excited levels therefore go through a maximum as the populating/depopulating mechanisms shift from the corona to the saturation balance. Because the plasma is more overpopulated in the lower levels during the prepeak than during the steady state, the negative glow is more ionizing in the former than the latter.

This shift in plasma properties from a very ionizing plasma in the prepeak to a lesser-ionizing plasma in the steady state also explains the underpopulation of upper levels in the former with respect to the latter.

As Fig. 7 demonstrates, while the space-charge factors greatly affect the distribution of states above the cathode darkspace, little effect is observed within the cathode darkspace. At 2 mm the after-peak/steady-state and after-peak/prepeak ratios are very similar for all the atom lines studied. This implies that the population of states does not change significantly between the prepeak and steady-state values. In the steady-state plasma, the applied field no longer decreases linearly between the two electrodes, but decreases almost entirely in the cathode fall (the distance between the cathode surface and the negative glow—usually ~ 0.5–2 mm) [68]. In addition to the reduced electron excitation effect in the cathode darkspace, excitation contributions from fast atom/ion collisions reduce the involvement of electron excitation in the population of states in this region. This implies that any vacillation in the electron excitation contribution to the population of states is less notable in the cathode darkspace than in the negative glow. This explains why, in Fig. 7 at 2 mm, the transformation between the prepeak and steady-state distribution of states is small and largely unaffected by the development of the negative glow.

The populations of states and the departure from TE conditions appear to be somewhat dependable on the plasma lifetime, or time-gated detection. Operating the PGD at shorter pulse widths, or collecting time-gated emission signals at shorter times, places the ionizing plasma further from TE conditions and preferentially populates the lower-lying levels while effectively attenuating emissions from the higher excited levels. Operating at longer pulse widths (> 4 ms), or time-gated monitoring at these longer times, encourages the formation of, and therefore emission from, the higher-level lines.

In agreement with the previous discussion, Yan et al. recently demonstrated that increasing the pulse width from 2 to 200 μs significantly affected the relative populations of various levels in the copper and argon atom and ion states [69]. The low-lying resonance state of copper was found to be the most enhanced in the prepeak relative to the steady-state domain, in agreement with the current findings. Unfortunately, Yan et al. only examined one line for each atom and ion in the plasma, so the distribution of excited states could not be confirmed as in agreement with those presented here.

3.5. Transition from an ionizing to a recombining plasma

The above discussion has shown that the distribution of excited states during the voltage-on period is heavily overpopulated in the lower levels with respect to the Boltzmann balance and underpopulated in the upper levels with respect to the Saha balance. These two observations are indications that the GD is dominantly ionizing while the voltage is applied [34–36]. If we assume that the electron temperature decays to the bath gas temperature when the voltage is removed [34,51] and that three-body (and possibly two-body) recombination is then possible, the plasma will transition to a recombining phase. In a recombining plasma, a downward flow of energy overpopulates the higher levels with respect to the Saha–Boltzmann balance. Fig. 6b shows examples of the populating mechanisms that are dominant at different electron densities in the recombining phase of plasmas.

At low electron densities, the capture radiative cascade (CRC) balance dominates and the density of (neutral) states is proportional to $p^{1.5}$ [34,35,37,38]. In this phase, depopulation is purely radiative. If the electron density exceeds the so-called Griem boundary [33], the depopulation of levels becomes collision-controlled. In this domain, the Saha–Boltzmann balance describes the higher levels and the saturation de-excitation balance describes the lower levels. Lower levels occupied by the saturation de-excitation balance are then populated proportional to p^{-6}. The boundary that distinguishes the de-excitation mechanisms of the higher and lower quantum levels is called the Byron boundary and is discussed in detail elsewhere [34,37]. It usually occurs around the sixth principle quantum number for a helium-like atom. Electron densities in the PGD used here are

expected to fall in the CRC zone, and therefore provide a population inversion in the after-peak related to $n(p)/g(p) \sim p^{1.5}$.

The after-peak/plateau emission ratios measured for the various excited levels of atoms demonstrate the diversity in the population of energy states between the ionizing and recombining phases of the plasma. When the electron density in the PGD is below 10^{10} cm^{-3}, the population of states in the ionizing and recombining phases will be proportional to $p^{-0.5}$ and $p^{1.5}$, respectively. The ratio of the after-peak/steady-state emission signals would then be expected to scale according to p^2, i.e. scale to the square of p. Fig. 4b and Fig. 5b suggest that the relationship between the after-peak/steady-state emission ratio and the energy levels (an approximation for the quantum levels) does indeed increase above a certain value energy ($\sim$15 eV for Ar I, $\sim$5.5 eV for Cu I), but the lack of data at higher energies prevents the determination of the exact relationship. This increase in the after-peak/plateau emission ratio for higher-lying states provides convincing evidence that recombination reactions between atomic ions and electrons in the CRC domain account for the majority of emissions occurring in the after-peak.

3.6. Mechanistic notes related to the source of the after-peak

In an effort to understand better the source of after-peak emissions, we refer to the CRC model developed by Fujimoto [37,38] (see Fig. 6). At the electron densities expected in this study ($\sim$10^{11} cm^{-3}) the plasma passes through a very interesting phase in the CRC diagram [37,38]: the 'cascade' contribution dominates the 'capture' contribution as a method of populating lower energy levels. For example, in hydrogen, radiative decay from the $p > 6$ levels is responsible for more than 90% of the populating mechanism for the $p = 5$ state. This implies that simple radiative decay from highly excited levels is increasingly important for the downward flow of energy exhibited in the after-peak. Also, because of a so-called bottleneck effect [34,37] caused by the slightly different de-excitation mechanisms above and below a critical quantum level (at $p \approx 6$), levels below this critical
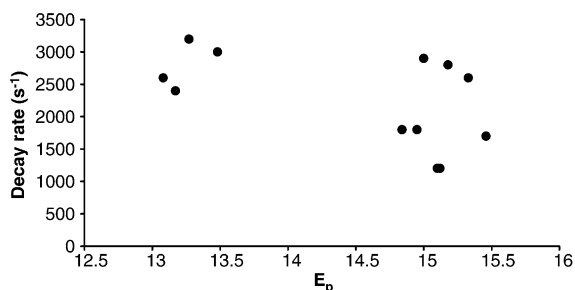

Fig. 8. Argon atom decay rates as a function of the upper energy level of the emitting species. Rates were determined from the plots of $\ln(I)$ vs. time between 5.4 and 7 ms and had minimum R^2 coefficients of 0.99, indicating first-order decay.

point will decay faster than levels above it. Remarkably, this phenomenon agrees, qualitatively at least, with the decay rates measured in Fig. 8, in which the lower levels ($E_p < 13.5$) decay at a slightly faster rate than the higher levels. These results suggest that the cascade contribution from highly excited states of Ar I are indeed largely responsible for the occurrence of the after-peak observed.

The argument for CRC involving argon ions in the after-peak is supported by many previous reports in the PGD literature. As Yan et al. demonstrated, the after-peak emission intensities increase as the pulse width increases [69]. Increasing the pulse width increases the number density of argon ions and therefore the probability of recombination in the after-peak. At pulse widths below 20 μs there is almost no notable after-peak for the Ar I or Cu I states. The after-peak becomes clearly visible at pulse widths longer than 50 μs. This argument is supported by the observations of other groups that after-peak emissions are typically not observed in discharges with pulse widths shorter than 50 μs [8,9,31,70–74], unless considerably higher powers are used to generate more charged pairs [59].

In agreement with Bogaerts and Gijbels [31,75], we find a disparity between the recombination rates observed in the PGD after-peak and the recombination rates predicted at an electron density of 10^{11} cm^{-3}. Assuming radiative (two-body) and three-body recombinations to be dominant, the

electron density would have to be taken as at least two orders of magnitude larger than expected in order reconcile the calculated recombination rates with our measured decay rates for the argon atom lines. The measured rates would require electron densities in the region of 10^{14} cm^{-3} (implying 1% ionization of Ar). As this is quite unlikely, this seems to indicate that either the electron density must dramatically increase at the onset of the afterglow, or that that an alternative mechanism must be responsible for the significant increases in the population of metastable argon atoms during the after-peak. Mason et al. recently performed some experiments with a flowing afterglow GD [76] and offered evidence for significant contributions from long-lived excited states of argon to metastable atom formation. These neutral states are speculated to be high-lying Rydberg states or auto-ionizing region (i.e. above the IP of Ar I) between 27 and 34 eV [77–82]. Mason et al. proposed that these levels could contribute to metastable formation (at 11.55 and 11.72 eV) via radiative or collisional decay and that the highly excited levels might be more quickly quenched by contaminant gases. The confirmation or refutation of the contributions of such states to the after-peak period of the PGD is something we plan to investigate further.

4. Conclusions

Characterization of the light emitted by excited argon and copper atoms and ions reveals the transient nature of the flow of energy in different regions of the plasma. Fast atom/ion collisions dominate the upward flow of energy to the lower energy levels within 0–2 mm of the cathode during the voltage-on period, but this mechanism is not significant for the higher excited states or in the negative glow (>3 mm). Electron excitation governs the latter region during the prepeak and steady-state regimes, but not to the same extent at each time. The development of space-charge effects as the plasma lifetime increases drives the lower levels from the corona balance towards the saturation balance, with the result that the lower levels are less populated in the steady-state than in the prepeak region. The growth towards the saturation balance later in the pulse lifetime enhances the population of levels closer to the IP. Factors such as the initial state of the gas, the method of energy deposition in the plasma, the loss of charged particles to the walls and the loss of radiation all contribute to deviations from TE and render an ionizing state in the plasma. The initial state of the gas is more influential at the pulse onset, which gives rise to the observed attenuation of higher lines and enhancement of lower lines.

Voltage termination results in electron thermalization and plasma recombination, demonstrated by the CRC flow of energy and population inversion in the after-peak. Levels closest to the IP become overpopulated with respect to TE conditions and cause a bottleneck effect in the downward flow of energy—meaning that the lower energy states depopulate more quickly than the higher energy states. Recombination effects are not observed close to the cathode, presumably because the electrons/ions diffuse to the cathode surface and are not available for recombination reactions.

Disparate behavior is found between the decay rates of optical emission lines measured here and the expected rates for recombination found in the literature. This difference can best be explained if high-energy Rydberg states or auto-ionizing states are available in sufficient numbers in the early after-peak region. Cascade contributions from these levels could presumably contribute to the after-peak observed, reducing the necessity for capture to take part in the CRC behavior of the after-peak.

The sputtered-atom excited states display very similar behavior to the bulk-plasma gas atoms, argon, and this has important ramifications for analytical applications. The judicious selection of the pulse width or time-gated selection and spatial position can significantly affect the absolute emission intensity and the attenuation of unwanted emission lines: shorter times promote lower energy transitions and longer times and the after-peak promote higher energy transitions.

Acknowledgments

this work. We also acknowledge the efforts of Dr Cris L. Lewis in data acquisition and in developing the macros utilized in data analysis.

References

[1] B. Chapman, Glow Discharge Processes, John Wiley and Sons, New York, 1980.

[2] W.W. Harrison, K.R. Hess, R.K. Marcus, F.L. King, Glow discharge mass spectrometry, Anal. Chem. A 58 (1986) 341A–356.

[3] D. Stuewer, Glow discharge mass spectrometry—a versatile tool for elemental analysis, Fresnius J. Anal. Chem. 337 (1990) 737–742.

[4] F.L. King, W.W. Harrison, Glow discharge mass spectrometry: an introduction to the technique and its utility, Mass Spectrom. Rev. 9 (1990) 285–313.

[5] R.K. Marcus, Glow Discharge Spectroscopies, 1st ed., Plenum Press, 1993.

[6] F.L. King, J. Teng, R.E. Steiner, Glow discharge mass spectrometry: trace element determination in solid samples, J. Mass Spectrom. 30 (1995) 1061–1075.

[7] C.M. Barshick, Glow discharge mass spectrometry, in: C.M. Barshick, D.C. Duckworth, D.H. Smith (Eds.), Inorganic Mass Spectrometry, Marcel Dekker Inc, New York, 2000.

[8] W. Hang, W.O. Walden, W.W. Harrison, Microsecond pulsed glow discharge as an analytical spectroscopic source, Anal. Chem. 68 (1996) 1148–1152.

[9] A. Bengston, C. Yang, W.W. Harrison, Microsecond pulsed glow discharge optical emission spectrometry—investigation of temporal emission characteristics, J. Anal. At. Spectrom. 15 (2000) 1279–1284.

[10] W. Hang, C. Baker, B.W. Smith, J.D. Winefordner, W.W. Harrison, Microsecond-pulsed glow discharge time-of-flight mass spectrometry: analytical advantages, J. Anal. At. Spectrom. 12 (1997) 143–149.

[11] W.W. Harrison, W. Hang, Powering the analytical glow discharge, Fresenius J. Anal. Chem. 355 (1996) 803–807.

[12] W.W. Harrison, W. Hang, Pulsed glow discharge time-of-flight mass spectrometry, J. Anal. At. Spectrom. 11 (1996) 835–840.

[13] J.B. Dawson, D.J. Ellis, Pulsed operation of hollow cathode lamps to increase the intensity of resonance lines for atomic absorption spectroscopy, Spectrochim. Acta A 23 (1966) 565–590.

[14] V. Majidi, M. Moser, C. Lewis, W. Hang, F.L. King, Explicit chemical speciation by microsecond pulsed glow discharge time-of-flight mass spectrometry: concurrent acquisition of structural, molecular and elemental information, J. Anal. At. Spectrom. 15 (2000) 19–25.

[15] G.P. Jackson, C.L. Lewis, S. Doorn, V. Majidi, F.L. King, Spatial, spectral and temporal characteristics of a millisecond-pulse glow discharge. Metastable argon atom production, Spectrochim. Acta B 56 (2001) 2449–2464.

[16] C.L. Lewis, G.P. Jackson, S.K. Doorn, V. Majidi, F.L. King, Spectral, spatial and temporal diagnostics of a millisecond-pulse glow discharge: copper atom and ion production, Spectrochim. Acta Part B 56 (2001) 487–501.

[17] C.L. Lewis, Dissertation, Department of Chemistry, West Virginia University, Morgantown, WV, 2001.

[18] P.W.J.M. Boumans, Understanding spectroscopy with a view to rationalizing spectrochemical analysis: an abysmal adventure or a realistic ideal?, Spectrochim. Acta Part B 46 (1991) 711–739.

[19] K. Rózsa, A. Gallagher, Excitation of Ar lines in the cathode region of a DC discharge, Phys. Rev. E 52 (1995) 913–918.

[20] A. Bogaerts, R. Gijbels, Behavior of the sputtered copper atoms, ions and excited species in a radio-frequency and direct current glow discharge, Spectrochim. Acta B 55 (2000) 279–297.

[21] A. Bogaerts, R. Gijbels, Description of the argon-excited levels in a radio-frequency and direct current glow discharge, Spectrochim. Acta Part B 55 (2000) 263–278.

[22] A. Bogaerts, R. Gijbels, J. Vlcek, Modeling of glow discharge optical emission spectrometry: calculation of the argon atomic optical emission spectrum, Spectrochim. Acta Part B 53 (1998) 1517–1526.

[23] A. Bogaerts, R. Gijbels, Fundamental aspects and applications of glow discharge spectrometric techniques, Spectrochim. Acta Part B 53 (1998) 1–42.

[24] A. Bogaerts, R. Gijbels, Modeling of glow discharge sources with flat and pin cathodes and implications for mass spectrometric analysis, J. Am. Soc. Mass Spectrom. 8 (1997) 1021–1029.

[25] C.M. Ferreira, J. Loureiro, A. Ricard, Populations in the metastable and resonance levels of argon and stepwise ionization effects in a low-pressure argon positive column, J. Appl. Phys. 57 (1985) 82–90.

[26] B.M. Jelenkovic, A.V. Phelps, Cathode fall-dominated Ar discharge: transient and steady-state experiments, J. Appl. Phys. 85 (1999) 7089–7096.

[27] S.W. Simpson, Ionization and recombination rates in argon plasmas, J. Phys. D: Appl. Phys. 22 (1990) 1161–1167.

[28] W. Vieth, J.C. Huneke, Studies on ion formation in a glow discharge mass spectrometry ion source, Spectrochim. Acta Part B 45 (1990) 941–949.

[29] K. Kano, M. Suzuki, H. Akatsuka, Spectroscopic measurement of electron temperature and density in argon plasmas based on collisional–radiative model, Plasma Sources Sci. Technol. 9 (2000) 314–322.

[30] C.V. Budtz-Jorgensen, J. Bottiger, P. Kringhoj, Energetic ion bombardment of the grounded anode in pulsed DC-glow discharges, Surf. Coat. Technol. 137 (2001) 104–110.

[31] A. Bogaerts, R. Gijbels, Modeling of a microsecond pulsed glow discharge: behavior of the argon excited levels and of the sputtered copper atoms and ions, J. Anal. At. Spectrom. 16 (2001) 239–249.

[32] H. Duncen, H.J. Tiller, J. Meisel, Uber ein verunreinigungsbedingtes nachleuchten bei einer glimmentladung durch Ar–H_2-mischungen, Spectrochim. Acta Part B 24 (1969) 632–634.

[33] J.A. Strauss, N.P. Ferreira, H.G.C. Human, An investigation into the role of metastable argon atoms in the afterglow plasma of a low pressure discharge, Spectrochim. Acta Part B 37 (1982) 947–954.

[34] J.A.M. van der Mullen, Excitation equilibria in plasmas: a classification, Phys. Rep. 191 (1990) 109–220.

[35] T. Fujimoto, Kinetics of ionization–recombination of plasma and population density of excited ions. I. Equilibrium plasma, J. Phys. Soc. Jpn. 47 (1979) 265–272.

[36] T. Fujimoto, Kinetics of ionization–recombination of a plasma and population density of excited ions. II. Ionizing plasma, J. Phys. Soc. Jpn. 47 (1979) 273–281.

[37] T. Fujimoto, Kinetics of ionization–recombination of plasma and population density of excited ions. IV. Recombining plasma—low temperature case, J. Phys. Soc. Jpn. 49 (1980) 1569–1576.

[38] T. Fujimoto, Kinetics of ionization–recombination of a plasma and population density of excited ions. III. Recombining plasma—high temperature case, J. Phys. Soc. Jpn. 49 (1980) 1561–1568.

[39] T. Fujimoto, Kinetics of ionization–recombination of a plasma and population density of excited ions. V. Ionization–recombination and equilibrium plasma, J. Phys. Soc. Jpn. 54 (1985) 2905–2914.

[40] J.A. Aparicio, J.A. del Val, V.R. Gonzalez, M.A. Gigosas, C. Perez, I. de la Rosa, S. Mar, Measurement of excitation equilibrium departure evolution in an argon pulsed plasma, J. Phys. Soc. Jpn. 68 (1999) 3885–3892.

[41] G.P. Jackson, Dissertation, Department of Chemistry, West Virginia University, Morgantown, WV, 2002.

[42] F.L. King, C. Pan, Temporal signal profiles of analytical species in modulated glow discharge plasmas, Anal. Chem. 65 (1993) 735–739.

[43] R.S. van Dyke, C.E. Johnson, H.A. Shugart, Phys. Rev. A 5 (1972) 991.

[44] A.V. Phelps, J.P. Molnar, Lifetimes of metastable states of noble gases, Phys. Rev. 89 (1953) 1202–1208.

[45] A.H. Futch, F.A. Grant, Mean life of the $^3P_2$ metastable argon level, Phys. Rev. 104 (1956) 356–361.

[46] E.A.H. Timmermans, I.A.J. Thomas, J. Jonkers, E. Hartgers, J.A.M. van der Mullen, D.C. Schram, The influence of molecular gases and analytes on excitation mechanisms in atmospheric microwave-sustained argon plasmas, Fresenius J. Anal. Chem. 362 (1998) 440–446.

[47] E.L. Bydder, G.P. Miller, A relaxation method for determining state of equilibrium and temperature ratio T_e/T_g in an argon ICPT, Spectrochim. Acta Part B 43 (1988) 819–829.

[48] F.H.A.G. Fey, W.W. Stoffels, J.A.M. van der Mullen, B. van der Sijde, D.C. Schram, Instantaneous and delayed responses of line intensities to interruption of the RF power in an argon inductively coupled plasma, Spectrochim. Acta Part B 46 (1991) 885–900.

[49] C. Kenty, The recombination of argon ions and electrons, Phys. Rev. 32 (1928) 624–635.

[50] J.A. Klinger, C.M. Barshick, W.W. Harrison, Factors influencing ion signal profiles in pulsed glow discharge mass spectrometry, Anal. Chem. 63 (1991) 2571–2576.

[51] M.A. Biondi, Studies on the mechanism of electron-ion recombination. I, Phys. Rev. 129 (1963) 1181–1188.

[52] M.A. Biondi, Diffusion, de-excitation and ionization cross sections for metastable atoms. I, Phys. Rev. 88 (1952) 660–665.

[53] A. Bogaerts, R. Gijbels, Modeling of metastable argon atoms in a direct-current glow discharge, Phys. Rev. A 52 (1995) 3743–3751.

[54] A. Bogaerts, R.D. Guenard, B.W. Smith, J.D. Winefordner, W.W. Harrison, R. Gijbels, Three-dimensional density profiles of argon metastable atoms in direct current glow discharge: experimental study and comparison with calculations, Spectrochim. Acta Part B 52 (1997) 219–229.

[55] A. Bogaerts, R. Gijbels, R.J. Carman, Collisional–radiative model for the sputtered copper atoms and ions in a direct current argon glow discharge, Spectrochim. Acta Part B 53 (1998) 1679–1703.

[56] D.A. Scott, A.V. Phelps, Excitation by fast atoms at very high electric field to gas-density ratios in argon, Phys. Rev. A 43 (1991) 3043–3055.

[57] C. Pan, F.L. King, Ion formation processes in the after-peak time regime of pulsed glow discharge plasmas, J. Am. Soc. Mass Spectrom. 4 (1993) 727–732.

[58] C.L. Lewis, E.S. Oxley, C.K. Pan, R.E. Steiner, F.L. King, Determination of $^{40}Ca^+$ in the presence of $^{40}Ar^+$: an illustration of the utility of time-gated detection in pulsed glow discharge mass spectrometry, Anal. Chem. 71 (1999) 230–234.

[59] A. Hirabayashi, Y. Nambu, M. Hasuo, T. Fujimoto, Emission spectroscopy of a pulsed helium-discharge plasma: transition from the ionizing phase to the recombining phase, Phys. Rev. A 37 (1988) 77–82.

[60] J.M. Brackett, J.C. Mitchell, T.J. Vickers, Temperature and electron density measurements in a DC glow discharge, Appl. Spectrosc. 38 (1984) 136–140.

[61] D. Fang, R.K. Marcus, Effect of discharge conditions and cathode identity on charged particle populations in the negative glow region of a simple diode discharge, Spectrochim. Acta Part B 46 (1991) 983–1000.

[62] D.M. Mehs, T.M. Niemczyk, Excitation temperatures in the hollow cathode discharge, Appl. Spectrosc. 35 (1981) 66–69.

[63] S.K. Ohorodnik, W.W. Harrison, Plasma diagnostic measurements in the cryogenically cooled glow discharge, J. Anal. At. Spectrom. 9 (1994) 991–996.

[64] D. Pollmann, K. Ingeneri, W.W. Harrison, Comparison of atomization and ionization in direct current, radiofrequency and microsecond pulse discharges, J. Anal. At. Spectrom. 11 (1996) 849–853.

[65] K. Tachibana, K. Fukuda, Population density and LTE of excited atoms in a positive column plasma. II. Measurement of argon, Jpn. J. Appl. Phys. 12 (1973) 895–902.

[66] J.A. Hornbeck, J.P. Molnar, Mass spectrometric studies of molecular ions in the noble gases, Phys. Rev. 84 (1951) 621–625.

[67] C.M. Barshick, D.H. Smith, E. Johnson, F.L. King, T. Bastung, B. Fricke, Periodic nature of metal–noble gas adducts in glow discharge mass spectrometry, Appl. Spectrosc. 49 (1995) 885–889.

[68] J.W. Bispham, Potential gradient in glow discharges from a point to a plane, Proc. R. Soc. Lond. A 8 (1908) 477–487.

[69] X. Yan, K. Ingeneri, W. Hang, W.W. Harrison, Factors influencing signal profiles in microsecond pulsed glow discharge atomic emission spectrometry, J. Anal. At. Spectrom. 16 (2001) 819–824.

[70] E. Oxley, C. Yang, W.W. Harrison, Quantitative depth analysis using microsecond pulsed glow discharge atomic emission spectrometry, J. Anal. At. Spectrom. 15 (2000) 1241–1245.

[71] E.H. Piepmeier, L. de Galan, Line profiles emitted by Cu and Ca hollow cathode lamps pulsed to one ampere, Spectrochim. Acta Part B 30 (1975) 263–279.

[72] Y. Su, P. Yang, Z. Zhou, X. Wang, F. Li, B. Huang, J. Ren, M. Chen, H. Ma, G. Zhang, Feasibility of applying microsecond-pulse glow discharge time-of-flight mass spectrometry in surface depth analysis, Spectrochim. Acta Part B 53 (1997) 1413–1420.

[73] C. Yang, K. Ingeneri, W.W. Harrison, A pulsed Grimm glow discharge as an atomic emission source, J. Anal. At. Spectrom. 14 (1999) 693–698.

[74] C. Yang, W.W. Harrison, Investigation of a novel hollow cathode configuration for Grimm-type glow discharge emission, Spectrochim. Acta Part B 56 (2001) 1195–1208.

[75] A. Bogaerts, R. Gijbels, G.P. Jackson, Modeling of a millisecond pulsed glow discharge: investigation of the after-peak, J. Anal. At. Spectrom., submitted for publication.

[76] R.S. Mason, P.D. Miller, I.P. Mortimer, Anomalous loss of ionization in argon–hydrogen plasma studied by fast-flow glow discharge mass spectrometry, Phys. Rev. E 55 (1997) 7462–7472.

[77] D. Lefaivre, P. Marmet, Electron excitation of Ar between 26 and 34 eV, Int. J. Mass Spectrom. Ion Phys. 18 (1975) 153–164.

[78] P. Veillette, P. Marchand, Photon detection of doubly excited states of argon produced by electron impact, Int. J. Mass Spectrom. Ion Phys. 18 (1975) 165–178.

[79] J.A. Simpson, G.E. Chamberlain, S.R. Mielczarek, Excitation of optically forbidden states in the ionization continuum by electron impact, Phys. Rev. A 139 (1965) 1039–1041.

[80] P. Marchand, J. Cardinal, Metastable yield of argon between 23 and 37 eV by electron impact, Can. J. Phys. 57 (1979) 1624–1633.

[81] X. Hua, J. Bai, L. Wang, 'Plasma' effect in the formation of long-lifetime Rydberg states, Chem. Phys. 270 (2001) 93–98.

[82] F.M.J. Pichanick, J.A. Simpson, Resonances in the total cross-section for metastable excitation of noble gases by electron impact, Phys. Rev. 168 (1968) 64–74.

[83] W.C. Martin, J.R. Fuhr, D.E. Kelleher, A. Musgrove, L. Podobedova, J. Reader, E.B. Saloman, C.J. Sansonetti, W.L. Wiese, P.J. Mohr, K. Olsen, 2002 National Institute of Standards and Technology, NIST, Gaithersburg, MD, 2002.